AIAA JOURNAL
Vol. 33, No. 5, May 1995

Near-Field Flow of Supersonic Swirling Jets

Andrew D. Cutler,* Brian S. Levey,† and Donna K. Kraus†
George Washington University/NASA/Joint Institute for Advancement of Flight Sciences, Hampton, Virginia 23681

The addition of swirl to scramjet fuel jets has been proposed as a method of enhancing fuel mixing, but little of a fundamental nature is known about supersonic swirling flows. Several jets with different amounts of swirl were created by tangential injection and acceleration through a convergent–divergent nozzle. The flowfields near the nozzle exit were investigated using pitot, cone, and total-temperature probes, and Rayleigh scattering from a laser light sheet. The results show that tangential injection is an efficient method for generating swirling jets, that the swirling jets mix much more rapidly with the stagnant air than comparable straight jets, and that, when overexpanded, turbulence is created in the jet core as a result of vortex breakdown. Mixing layer growth rates are shown to correlate with Richardson number.

Introduction

THIS work is motivated by the desire to design more efficient fuel injectors for supersonic combustion ramjet (scramjet) engines. The fuel for these engines, probably hydrogen, will be used to cool the aerodynamic surfaces prior to combustion. A significant contribution to the thrust of the engine can be obtained if the hot fuel is injected into the engine as a jet with a large component parallel to the airstream. However, with parallel injection the mixing of fuel and air is poor, particularly at the speeds associated with scramjet combustors. Studies have shown that the growth rate of a two-dimensional shear layer depends primarily upon the convective Mach number M_c, defined as the characteristic Mach number of the eddies relative to the low-speed stream, or as the Mach number of the high-speed stream relative to these eddies.[1–3] In the convective Mach number range between about 0.25 and 1.0, shear-layer growth rate falls to 20–40% of that of a similar incompressible shear layer, and thereafter appears to remain constant. Therefore, in order for the combustor to be of reasonable length and to simultaneously achieve complete mixing and combustion, methods for enhancing the mixing are required. One method to increase mixing of a fuel jet is to add swirl to it; swirl, essentially the addition of mean-streamline curvature, increases mixing-layer growth rates.[4–8] Addition of swirl may also lead to vortex breakdown,[9–13] and it may be assumed that because vortex breakdown typically leads to turbulence generation in the core of the vortex, breakdown will lead to increased jet/air mixing.

The effect of streamline curvature on shear-layer stability was investigated by considering the motion of a fluid particle displaced normal to the mean streamline in such a way that its moment of momentum and entropy are preserved.[6] In a low-speed flow of uniform composition the stability was given simply by the gradient of circulation, so that the core of a turbulent vortex is curvature stabilized and the shear layer between a swirling jet and an irrotational parallel flow is destabilized. The effect of positive radial density gradient was shown to be stabilizing (e.g., in the case of a light-gas jet into air), the situation being analogous to that in a buoyancy stabilized stratified flow. At high Mach numbers, the effect of the radial density gradient was shown to be offset by an effect of Mach number so that, if the flow is irrotational and of uniform composition and entropy, the flow is neutrally stable. A temporal linear stability analysis for a self-similar compressible swirling jet, with the ratio of maximum tangential velocity to maximum axial velocity less than 0.1 and the Mach number less than 1.4, into stagnant surroundings, has indicated large effects of swirl.[7] Negative azimuthal wave numbers were much more unstable than for a similar nonswirling jet, and the normally stabilizing effect of high Mach numbers was greatly reduced by the addition of swirl. Experimental work at Pennsylvania State University[4,5] and NASA Langley (to be reported here) has shown that, whereas mixing-layer growth rates in nonswirling jets are reduced substantially as convective Mach number rises, the increase in growth rate due to swirl is not diminished by compressibility. This has been attributed to the effects of three dimensionality[5]; unlike spanwise structures, which characterize mixing in two-dimensional, incompressible shear layers, oblique or streamwise structures are not diminished by the effects of compressibility. Streamwise structures (e.g., Taylor–Görtler vortices) are, of course, a characteristic of turbulent shear layers destabilized by the effects of curvature. Historically, the stability effects of curvature have been characterized by the gradient or the flux Richardson number,[8] but no attempt has previously been made to correlate the effects of swirl upon mixing-layer growth rate in terms of a Richardson number.

Vortex breakdown has been extensively studied in low-speed flows, and the reader is referred to one of the many review articles on the subject (e.g., Ref. 9). It occurs when the ratio of maximum tangential velocity to freestream axial velocity in the vortex is increased by an adverse streamwise pressure gradient so that it exceeds some threshold value (of order 1). Breakdown is usually associated with an abrupt expansion of the vortex core, accompanied by a stagnation point and a region of recirculation, and instability to small perturbations is greater downstream. Studies of supersonic vortices and swirling jets show that breakdown can occur as a result of interaction with a shock wave,[10–13] which, of course, produces severe adverse streamwise pressure gradients. The shock wave that initiates the breakdown is deflected forward by the region of recirculation, the region acting like a bluff body, creating a "bubble" shock.[12]

The work presented here is an experimental study of a supersonic, swirling air jet discharging into stagnant air. This configuration was chosen because it is simple, instrumentation access is straightforward, it is of fundamental interest, and it is relevant to scramjet fuel mixing. The flow in the immediate vicinity of the nozzle exit was investigated providing both fundamental information on the effect of swirl on mixing-layer growth rate and information on supersonic vortex cores and vortex breakdown. The flow downstream of the point where the mixing layers penetrated to the jet axes was not considered; presumably the flow becomes subsonic here, approaching the self-similar low-speed form which has been extensively studied.

Experimental Method

The swirling jet facility is illustrated in Fig. 1. High-pressure air was injected at low speed ($M < 0.2$) from the large plenum through up to 96 tangentially drilled holes into the swirl chamber. The air was then accelerated through a 2:1 exit to throat area ratio

Received March 21, 1993; revision received Aug. 24, 1994; accepted for publication Aug. 28, 1994.

*Assistant Professor, School of Engineering and Applied Science. Senior Member AIAA.

†Graduate Research Scholar Assistant, School of Engineering and Applied Science. Student Member AIAA.

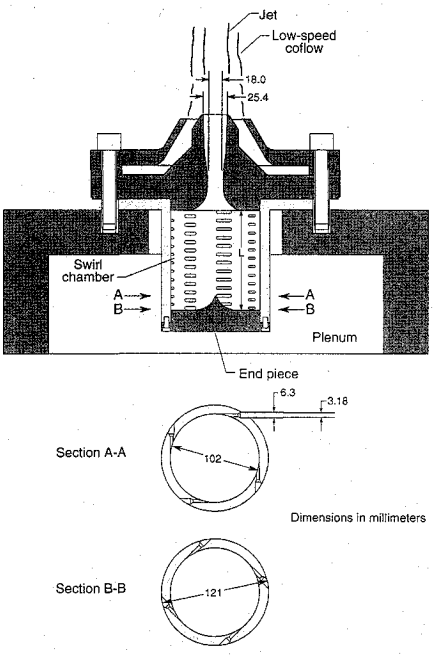

Fig. 1 Swirling jet generator with coflow nozzle in place.

convergent–divergent nozzle with exit diameter d_j 25.4 mm. By interchanging end pieces the length of the swirl chamber, L, and consequently the number of injection holes, could be varied. Decreasing the number of the injection holes increased the tangential velocity of injection, thus increasing the swirl. By removing the end piece altogether the jet could be run without swirl. Three cases were considered: straight (no swirl); low swirl, where $L = 114$ mm so that all 96 holes were exposed (a total injection area of 760 mm^2), and high swirl, where $L = 19$ mm so that 16 holes were exposed (a total injection area of 127 mm^2). The swirl number for these cases, defined in the conventional manner as the ratio of the total streamwise convection rate of angular momentum to the total streamwise convection rate of streamwise momentum, was computed from probe measurements (to be discussed) to be 0, 0.27, and 0.39, respectively. Wall pressure taps were located in the plenum, in the swirl chamber, at the throat, and at the exit of the nozzle, and a thermocouple probe was located in the plenum. A concentric nozzle mounted around the jet nozzle is shown in the figure; dry air from the same source as the main jet was introduced into this nozzle through four tubes, providing a low-speed coflow. This nozzle was absent (i.e., no coflow) for the probe tests and for visualization of the mixing layer, but was present for visualization of the jet to eliminate water condensation in the jet/air mixing layer (to be discussed). Total temperature of the compressed air supply varied somewhat during a run but was in the range of 283–298 K. For the straight jet case (nominal Mach number of 2.2) with exit pressure matched to atmospheric, the Reynolds number based on jet diameter was 294,000.

Measurements of flow direction, Mach number, total pressure, and total temperature were made along the diameter at an axial distance from the exit plane of $x/d_j = 0.31$ using a cone probe, a five-hole probe, and a temperature probe. The flow in a plane through the axis of the jet, from $x/d_j = 0.063$ to 2.13, was visualized by imaging of Rayleigh scattering from a laser-light sheet.

Probe Measurements

The cone probe was a nominal 10-deg semivertex angle cone with four symmetrically placed static taps of 0.15 mm diam placed 1.83 mm from the tip. The five-hole probe was constructed of five small stainless-steel tubes of 0.13–0.15-mm i.d., a central one and four others symmetrically spaced around it, packed inside a 1.27-mm o.d. tube with the gaps between the tubes filled and the tip machined to form a 25-deg semivertex angle cone. The temperature probe consisted of a commercial miniature thermocouple, the junction of which was located at the tip of a 0.20-mm-diam needle. The 0.02-mm thermocouple wires passed through the core of the needle, which was quartz with a steel cladding, and the needle was incorporated into a conventional shrouded probe of outside diameter 0.76 mm. Each probe was mounted in a motorized traversing mechanism which translated the probe along the diameter, and yawed it in the plane of the diameter and the jet axis. The five-hole probe was mounted so that two of the four side holes were in the plane of yaw. Data acquisition and control of the traversing mechanism was by a personal computer.

The aerodynamic symmetry and angular sensitivity of the five-hole probe was checked by a yaw calibration on the axis of the straight jet (matched exit pressure). The pressures from the side tubes in the yaw plane were found to depend roughly linearly and symmetrically upon yaw angle in the range ± 10 deg. The out-of-plane side tube and center tube pressures were almost independent of yaw angle in the same range. The temperature probe was insensitive to yaw misalignment. The recovery factor measured in the straight jet referenced with a thermocouple in the plenum was about 99%; thus, no correction for recovery factor was applied to the data.

The helix angle of the flow [$\alpha \equiv \tan^{-1}(v_\theta/u)$, where v_θ is the tangential velocity component and u is the axial velocity component] was found to the nearest degree by yawing the five-hole probe so as to minimize Δp, the pressure difference between the yaw-plane side tubes. Δp was then measured at ± 5 deg from this position, and the three readings interpolated to zero Δp to obtain a final flow angle. The angle measurements were referenced to the flow at the centerline of the straight jet. Pitot pressure was obtained from the center tube of the five-hole probe. Cone pressure and total temperature measurements were made with the probes aligned in yaw using previous measurements of α. The radial angle of the flow [$\beta \equiv \tan^{-1}(v_r/u)$, where v_r is the radial component of the velocity] was estimated from measurements of the pressure difference between the two side tubes lying in the radial plane to be less than ± 4 deg. Thus, the pitot pressure, cone pressure, and temperature measurements were not significantly affected by misalignment with the flow.

Total pressure and Mach number were obtained from pitot and cone pressure measurements. The Rayleigh supersonic pitot formula (which relates pitot pressure to static pressure and Mach number), tables of cone surface pressure coefficients as a function of cone angle and Mach number, and simple isentropic relations were used to solve for total pressure, static pressure, and Mach number. The cone angle was found by calibration in the straight jet where the pitot pressure, total pressure (assumed equal to the plenum pressure), and cone pressure were all known. The calibrated angle of 10.6 deg was close to the actual angle measured under a microscope, which was 10.4 deg.

Uncertainties (at 20:1 odds) in the directly measured quantities are as follows: ± 1 deg in flow yaw angle including the effect of uncertainty in the zero position, $\pm 0.5\%$ of full scale in probe pressure, and $\pm 1\%$ in absolute total temperature including the effect of recovery factor. Uncertainty in calibration cone angle, which includes the sensitivity to uncertainty in individual pressure measurements obtained by perturbation analysis, is ± 0.5 deg. Mild asymmetry in the probe data was observed in the cases with swirl, which may have been due in part to positional error and/or to probe interference with the flow. (The discrepancy between the measurements at equal distances either side of the axes from the average was treated as an uncertainty.) Uncertainties in derived quantities obtained by perturbation analysis, including the effects of all of the individual sources of uncertainty, are shown by error bars in the figures. In some cases these are high, mostly because of the effect of asymmetry.

Rayleigh Scattering Imaging

The experiment employed a frequency quadrupled Nd:YAG laser which was pulsed at 10 Hz (10-ns pulsewidth) and provided output energy of about 20–30 mJ per pulse at 266 nm. A pair of cylindrical lenses and a spherical lens were used to form the light sheet. The theoretical (diffraction limited) light-sheet thickness was about 50 μm, although the actual light sheet was probably thicker. The Rayleigh scattered light was imaged by an intensified video (RS170) charge-coupled-device camera through an F4.5, 105-mm focal length uv

camera lens, and was electronically shuttered with a gate width of about 5 μs for rejection of background light. The intensified video camera was tested for linearity and was found to be linear to within 5% of full scale. The video images were digitized by a personal computer equipped with a frame grabber. Images of the flowfield were normalized with a reference image to correct for nonuniformities in the detector gain and light sheet, and both flowfield and reference images were corrected for background light and camera zero offset by substraction of a background image. Single images were noisy as a result of low-light levels (shot noise) and noise introduced by the intensifier. In the images presented here, signal-to-rms-noise ratio is roughly 14 times the square root of density normalized by atmospheric density. The Rayleigh scattering experiment was initially attempted with light at 532 nm rather than 266 nm, which allowed a slightly simpler optical layout. However, at 532 nm the light scattering from small particles of dust (which are unavoidably present in the compressed air) is prohibitively high relative to scattering from air or from condensation clusters (which lie in the Rayleigh range). This is because scattering from the large particles in the Mie-scattering range is roughly wavelength independent whereas Rayleigh scattering depends upon wavelength to the minus fourth power.

Typical supersonic wind tunnels are commonly operated at low-static temperatures, and the air is, thus, supersaturated with water vapor and/or with carbon dioxide. Some degree of supersaturation can be tolerated before condensation occurs, and whether or not condensation actually occurs is somewhat unpredictable. If it does occur, the scattering from the condensate tends to dominate the molecular Rayleigh scattering. In our experiment the jet air had 3–10 ppm of water at the compressor station, greatly exceeding the saturated condition (about 5×10^{-5} ppm for the straight jet with matched exit pressure). In practice we found that condensation of water vapor occurred in the mixing layer of the jet due to entrainment of humid stagnant air. The condensation clusters are small enough to follow the flow and form fairly quickly, thus they provide a good method for visualizing the mixing layer. (See Ref. 14 for a similar experiment using alcohol condensation.) Condensation of water in the mixing layer could be eliminated for a short streamwise distance by providing a low-speed coflow of dry air (the coflow Mach number ranged from $M \approx 0.05$ for the straight case to $M \approx 0.15$ for the high-swirl case), so that dry rather than humid air was entrained by the mixing layer. (This coflow had no effect on the fluid mechanics of the jet except that it altered the water content of the mixing layer.) It was then possible, in certain cases, to obtain images of molecular Rayleigh scattering uncontaminated by scattering from condensation.

Results

The plenum pressure was increased in steps up to 550 psia for each of the swirl cases and pressures in the plenum, p_0, and on the nozzle wall close to the exit, p_e were measured. As the plenum pressure rose, with chocked flow in the nozzle, the ratio p_e/p_0 fell until the nozzle was shock free, after which this ratio remained constant. This fall was quite rapid in the straight jet and low-swirl cases, but more gradual for the high-swirl case, and constant p_e/p_0 was reached at $p_0/p_{0,m}$ (where $p_{0,m}$ is the plenum pressure at which the exit pressure was matched to atmospheric pressure) of 0.55, 0.61, and about 0.64 for the straight, low-swirl, and high-swirl cases respectively. Throat and exit pressure measurements and comparisons with a simple calculation of the flow of an isentropic, irrotational vortex in the nozzle are given in Ref. 15. All of the cases considered in this paper are for supersonic, shock-free flow in the nozzle.

Nozzle Exit Profiles

Some of the pressure and temperature probe measurements, and quantities derived from these measurements, are shown in Fig. 2. Figure 2a shows the tangent of the helix angle for low and high swirl and a fit to the function K/r in the outer part of the jets (K is -0.144 for low swirl and -0.209 for high swirl); the fits in this region are both reasonable. The streamwise velocity normalized by the sonic speed of sound, $M_x^* \equiv u/a^*$, is constant across the diameter and equal to 1.75 (with uncertainty of ± 0.1 in the outer region, greater in the core) for all three cases. The total pressure, shown in Fig. 2b,

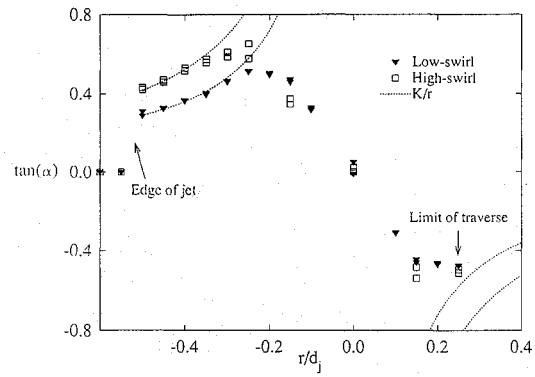

a)

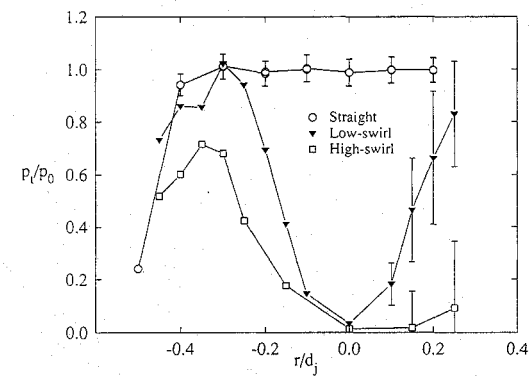

b)

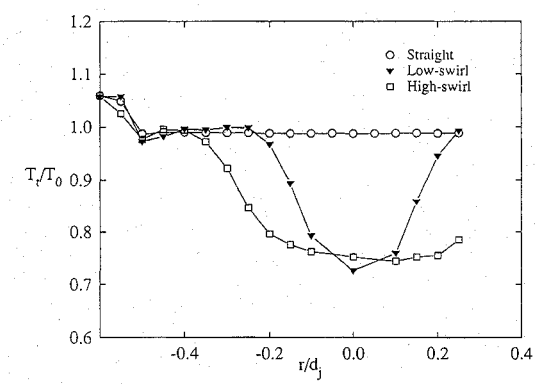

c)

Fig. 2 Mean flowfield quantities derived from probe measurements at $x/d_j = 0.31$: a) tangent of flow helix angle, b) total pressure, and c) total temperature.

is also roughly constant in this outer region, and so the swirling jets are approximately irrotational in the mean there; the straight jet is of course completely irrotational (excluding the boundary layer). In (hypothetical) purely irrotational compressible vortices the Mach number rises toward the center due to the increase in the tangential component of velocity, tending toward infinity at some finite radius; within this radius the pressure and density are zero, i.e., there is no flow. Thus, given $v_r = 0$, then $v_\theta r$ (where r is the radial coordinate) and u are constant, and at the $M \to \infty$ radius we get

$$\frac{v_\theta}{u} = \left[\left(\frac{\gamma+1}{\gamma-1}\right)\frac{1}{M_x^{*2}} - 1\right]^{\frac{1}{2}}$$

In practice, the effects of viscosity prevent this infinite Mach number condition from being reached, and a zero pressure and density core is not obtained. In the current experiment the peak v_θ/u is 0.51 for the low-swirl case and 0.58 for the high-swirl case, which is 0.52 and 0.59, respectively, of this inviscid limit. In previous experimental studies of high-speed vortex flows, where turning vanes or wings in

the nozzle generated the swirl,[4,11,12] the maximum v_θ/u achieved did not exceed about 0.3 of this limit. As a consequence of this close approach to the irrotational vortex, core minimum pressures and densities are lower in our study than in previous studies.

The data in Fig. 2b is unreliable in the core for the swirling cases, as indicated by the error bars, but it does seem to show that total pressure in the swirling jet cores is very low, as of course is the static pressure and density (not shown). Total temperature normalized with plenum temperature, shown in Fig. 2c, is slightly greater than 1 in the outer part of the swirling jets but falls to 0.70–0.75 in the cores. A similar separation of energy has been observed for compressible flow in vortex tubes (e.g., Ref. 16); these devices consist of tubes into which gas is injected tangentially and from which lower total temperature fluid is extracted near the axis. In Ref. 17, a mathematical model of the flow in a vortex tube was postulated which was able to explain this energy separation. Since the swirl chamber of the present facility is just such a device, it should not be surprising that such low-core total temperatures are observed in our experiment. A much smaller drop in total temperature at the axis to 0.95 of the peak was observed in the $M = 3$ swirling jet in Ref. 12, which was generated by vanes rather than by tangential injection and which had lower peak tangential velocities. Therefore, it seems likely that some degree of energy separation occurs in any supersonic vortex, however generated.

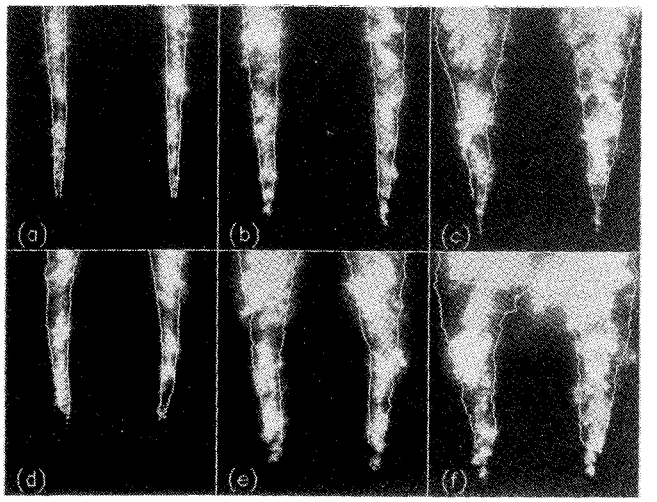

Fig. 3 Planar images of mixing-layer condensation in nonswirling and swirling jets: a) straight, $p_0/p_{0,m} = 0.99$, b) low swirl, $p_0/p_{0,m} = 0.98$, c) high swirl, $p_0/p_{0,m} = 1.0$, d) straight, $p_0/p_{0,m} = 0.60$, e) low swirl, $p_0/p_{0,m} = 0.60$, and f) high swirl, $p_0/p_{0,m} = 0.68$.

Mixing-Layer Development

Figure 3 shows single-shot images of scattering from the laser-light sheet for various pressure-matched and over-expanded cases. Superimposed on these images are lines of 35% intermittency, as described subsequently, which mark the inner and outer edges of the mixing layer. It is immediately evident from them that swirl produces a substantial increase in mixing-layer growth rate, and also, to a lesser extent, so does the reduction of jet pressure. The eddy structures in the mixing layer are less flattened with the swirling (and pressure mismatched) jets, but they are no more periodic or organized in their appearance. The effect of swirl is believed to be due to destabilization by curvature and is correlated later with the Richardson number. The effect of pressure mismatch is probably due to a combination of the following: turbulence generation through the interaction of the mixing layer with the shock wave emanating from the nozzle lip, a reduction of convective Mach number downstream of the shock, and, in the case of the swirling jets, vortex breakdown in the core of the jet resulting in turbulence generation there. No effort will be made to correlate growth rates with these phenomena, but the phenomena themselves will be discussed further in relation to the density imaging.

Previous workers have used flow visualization to obtain mixing-layer "visual" growth rates: for example, in Ref. 1 schlieren was used to obtain them in a two-dimensional mixing layer and in Ref. 3 condensation imaging was used in an axisymmetric mixing layer. Visual growth rates were obtained by drawing (by eye) mean straight-line tangents to the edge of the mixing layer. It was difficult to obtain consistent results in the present study by drawing straight-line tangents because of the relatively small number of eddy structures in the field of view. We obtained mixing-layer growth rates from distributions of intermittency, defined as the probability of the presence condensation (i.e., a mixture of jet and atmospheric air in any nonzero/noninfinite proportion) at any given point. The brightness of the scattering from the condensation increased in the downstream direction, presumably because the condensation particles took time to build up in size and number once conditions were favorable for their development (i.e., where humid atmospheric and cold jet air had mixed). To provide a first-order correction for this lag, pixel values in each pixel row of an image were corrected by dividing by the peak pixel value in the corresponding row of a 46 image average, thus enhancing the fainter part of the mixing layer near the jet exit. (Note that the images presented in Fig. 3 have already been corrected in this manner.) This correction is exact if the mixing layer is self-similar, which is unlikely to be the case very close to the nozzle exit and, in fact, the correction fails in this region due to absence of condensation. However, the mixing-layer growth rates ultimately derived from the corrected data were based on data farther downstream and are unlikely to be affected by lack of similarity. After this correction was applied, each image was thresholded so that pixels with image intensity greater than 20% of full scale were assigned a value 1 and remaining pixels were assigned 0. An intermittency image was then obtained by averaging 46 such thresholded images. Lines of constant intermittency were reasonably well approximated by straight lines intersecting at the nozzle exit; mixing-layer growth rates δ' were, therefore, obtained by finding the radial distance between the occurrence of a specified intermittency level on the left-hand and right-hand side of each mixing layer at $x/d_j = 2.1$ and dividing it by x. The results for the left-hand and right-hand side mixing layers of each case were then averaged. The growth rates presented here were evaluated using the 35% intermittency level because the resulting growth rate for the straight jet then agreed with visual growth rates obtained in previous experiments on (nonswirling) mixing layers with similar convective Mach numbers ($M_c = 0.92$) (Refs. 1 and 3). The growth rates with matched exit pressure cases were 0.082, 0.15, and 0.28 for the straight, low-swirl, and high-swirl cases, respectively.

The (gradient) Richardson number is defined as[6,8]

$$Ri = \left[\frac{v_\theta^2}{r^2}\left(\frac{2}{v_\theta}\frac{\partial v_\theta r}{\partial r} + \frac{r}{\rho}\frac{\partial \rho}{\partial r} - M_\theta^2\right)\right] \Big/ \left[\left(\frac{\partial v_\theta}{\partial r}\right)^2 + \left(\frac{\partial u}{\partial r}\right)^2\right]$$

where M_θ is the Mach number based on v_θ and ρ is density. If $Ri < 0$, then the effect of curvature is to destabilize the mixing layer, and if $Ri > 0$, the effect is to stabilize it. The radial distributions of u, v_θ, and ρ in the mixing layer were not measured and, for the purposes of estimating Ri, have been modeled analytically. Consider for a moment the general case of a swirling jet (stream 1) of a gas A with a nonswirling coflow (stream 2) of gas B. It can be shown that, if some simple assumptions can be made, the nondimensional profiles of velocity, stagnation enthalpy, and species mass fraction are the same, i.e., $[u(y)-u_2]/(u_1-u_2) = v_\theta(y)r/(v_\theta r)_1 = [H(y)-H_2]/(H_1-H_2) = m_A(y) = 1-m_B(y)$, where $y \equiv r - d_j/2$, H is the total enthalpy, and m_A and m_B are mass fractions of gas A and gas B, respectively. The assumptions are as follows: the streamwise pressure gradient in the mixing layer is zero, the mixing layer is fully turbulent, the presence of the viscous core in the swirling jet does not affect the development of the mixing layer, the origin of the mixing layer and the total shear layer are the same, the mixing layer is a thin shear layer, and turbulent Prandtl and Schmidt numbers are equal to one. The turbulent Prandtl/Schmidt number unity assumption is

$$\frac{\overline{u'v'_r}}{\partial u/\partial y} = \frac{\overline{v'_\theta v'_r} r}{\partial v_\theta r/\partial y} = \frac{\overline{T'v'_r}}{\partial T/\partial y} = \frac{\overline{m'_A v'_r}}{\partial m_A/\partial y}$$

The Richardson number at the center of the mixing layer ($y = 0$) was

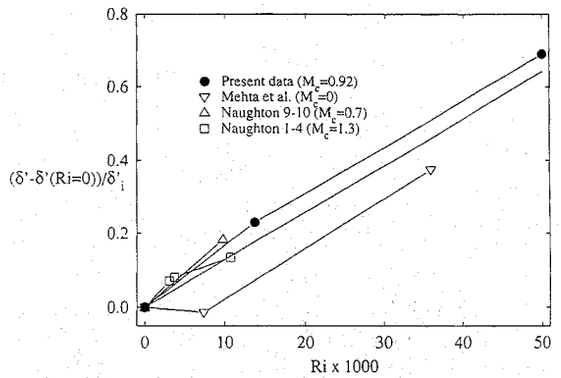

Fig. 4 Normalized mixing layer growth rate as a function of Richardson number.

obtained from the experimental molecular weight, composition of gases A and B , velocities u_1, u_2, $(v_\theta r)_1$, total enthalpies H_1 and H_2, and thickness δ by modeling these nondimensional profiles with the function $\frac{1}{2}[1 - \text{erf}(2y\sqrt{\pi}/\delta)]$. This was done for the present cases, and also for the Naughton[4] cases 1–4 (pressure-matched $M_1 = 3$ helium jets into $M_2 = 4$ air coflow) and cases 9–10 (pressure-matched $M_1 = 2.8$ helium–nitrogen jets into $M_2 = 4$ air coflow), and the data of Mehta et al.[18] (low-speed swirling air jets into air). In both the data from the literature and the present data, δ' was computed assuming linear growth from the nozzle exit at $x = 0$ to the farthest downstream experimental point at $x = X$, the δ used was found at the midpoint of this range with the equation $\delta \approx \delta' X/2$.

The mixing-layer growth rates normalized by the incompressible growth rates (δ_i', computed using the equation of Ref. 1) and referenced to the corresponding ratio with no-swirl are plotted vs Richardson number in Fig. 4. The results show that the growth-rate increment due to swirl correlates well with Richardson number, suggesting that the effect of swirl on mixing is indeed due to the curvature instability. A least-squares fit to the data gives the equation $[\delta' - \delta'(Ri = 0)]/\delta_i'(Ri = 0) = 13Ri$. The results show some scatter, due in part to experimental error, but the scatter may also, in part, be explained by the assumptions made in obtaining the Richardson number. The most questionable assumption, especially in the case of the Naughton[4] data, is that the mixing layer and the shear layer had the same origin; in fact, the boundary-layer thickness of the coflow stream at the jet nozzle exit was rather large in this case and was included in the measurement of visual thickness. Also, the assumption of no effect of the core may have been incorrect since, in many cases, the mixing layer and the core had merged at the downstream end of the range of the fits; indeed, the Mehta et al.[18] case had no irrotational region of the jet at all, but rather, the jet approximated solid body rotation. Another questionable assumption made in obtaining the mixing-layer growth rates was that the growth rate was a constant with respect to streamwise distance; in fact, the dependence of Richardson number up δ implies that δ' is a function of x. Notwithstanding these problems, the trends of the results seem unmistakable. A final, important result which comes from this analysis is that the stabilizing effects of composition gradient in swirling light-gas jets are not very large. In the Naughton[4] cases (for helium jets) the second and third terms (density gradient and tangential Mach number terms) in the numerator of the equation for $Ri(y = 0)$ summed together were of positive (stabilizing) sign but amounted to no more than about 30% of the (destabilizing) angular momentum gradient term.

Density Imaging

Figure 5 shows single-laser-pulse images for (almost) the same pressure cases as in Fig. 3 with a low-speed coflow of dry air provided to eliminate condensation in the mixing layer. In all cases this allows regions of molecular Rayleigh scattering, where intensity is proportional to gas density, to be seen. However, in some cases there are also regions where scattering is still dominated by condensation; at the top of Figs. 5e and 5f, and at the top right of Figs. 5b and 5c there is scattering due to condensation of water from entrained humid air, the jet has mixed through the dry-air coflow

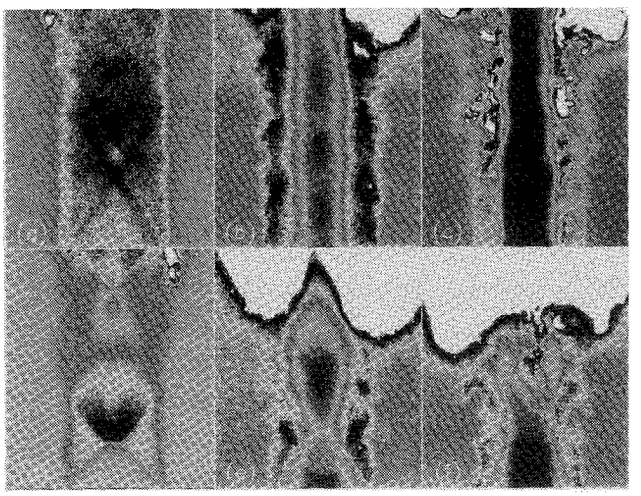

Fig. 5 Planar images in nonswirling and swirling jets with low-speed coflow: a) straight, $p_0/p_{0,m} = 1.0$, b) low swirl, $p_0/p_{0,m} = 1.0$, c) high swirl, $p_0/p_{0,m} = 1.0$, d) straight, $p_0/p_{0,m} = 0.61$, e) low swirl, $p_0/p_{0,m} = 0.61$, and f) high swirl, $p_0/p_{0,m} = 0.68$.

at these locations. Also, in Fig. 5c, for the pressure-matched, high-swirl case there appears to be condensation around the periphery of the jet core, close to the maximum Mach number radius—this is attributed to condensation of water, or possibly carbon dioxide, occurring within the jet air itself as some temperature-pressure threshold is crossed (the high-swirl case has the highest peak Mach number, hence the lowest minimum temperature). The presence of this condensation, the relatively poor single-to-noise ratio, and the probable presence of uncorrected background single make quantitative interpretation of these images problematic. However, as a means of flow visualization they are informative.

It is evident from Figs. 5b and 5c that the pressure-matched swirling jets are stable in the core region, and, but for the growth of the mixing layer, would probably maintain themselves for a considerable streamwise distance. Similar behavior is observed in low-speed trailing vortices and may be explained by the effects of curvature; $\partial(v_\theta r)/\partial r$ and, consequently, Richardson number are positive, hence stabilizing, in the core. However, there is some waviness in the core (a slight periodic variation in core diameter) due, perhaps, to propagation and reflection of weak shocks originating at the nozzle exit or to the influence (through the pressure field) of the mixing-layer eddies. In the overexpanded cases a conical shock is formed which emanates from the nozzle lip. For low swirl (Fig. 5e) this leads to an axisymmetric bubble shock which propagates forward of the (projected) apex of the cone and intersects the axis at $x \sim 0.25d_j$. Inspection of images taken at different times shows the bubble shock to be quite unsteady. A second such shock can be observed which intersects the axis about $1.25d_j$ farther downstream which is much more unsteady, both in location and strength (both shocks are more clearly visible in schlieren images not shown here). Similar bubble shock systems have been reported previously and are believed to be due to the presence of vortex breakdown.[10–13] For high swirl (Fig. 5f) there is no bubble shock, but intermittent "tongues" of condensation, which extend upstream along the axis, indicate the existence of intermittent reversed flow. The presence of water condensation in the core, which occurs for both overexpanded swirling cases at the top of the field of view, indicates that some small quantity of humid stagnant air has been entrained into the core and, therefore, that the core downstream of breakdown is turbulent.

In addition to the swirling cases with $p_0/p_{0,m} = 1.0, 0.61$ (low swirl), and 0.68 (high swirl) shown here, swirling cases with $p_0/p_{0,m} = 0.88$ and 0.75 (both low and high swirl) were investigated. In these cases, the conical shock which emanates from the nozzle lip leads to a constriction (reduction in diameter) of the core (only slight at $p_0/p_{0,m} = 0.88$, but more noticeable at $p_0/p_{0,m} = 0.75$, both cases). However, the conical shock is weaker and does not lead to the formation of a bubble shock, and there is

no evidence of reversed flow on the jet axis. It seems that the vortex breakdown behavior of both low- and high-swirl jets is quite similar, with breakdown being present for (roughly) $p_0/p_{0,m} < 0.7$. This result (in conjunction with the peak v_θ/u results given earlier) allows the correlation of vortex breakdown with shock pressure ratio and peak v_θ/u given in Refs. 11 and 12 to be extended to higher peak v_θ/u.

Conclusions

Three air-in-air jets have been studied whose axial velocity was similar, but whose tangential velocity distribution differed: a straight jet ($M \approx 2.2$) and two swirling jets. Swirl was generated using tangential injection into a plenum chamber ahead of a convergent–divergent nozzle. Pressure and temperature probe measurements at the jet nozzle exit showed that the swirling jets had higher peak helix angles than in previous experimental studies where the swirling jets or vortices were generated by wings or vanes in the nozzle. The jet mixing layers were visualized using planar imaging of condensation, and it was found that growth rates were increased substantially by swirl. The effects of swirl were shown to correlate with Richardson number, indicating that the increase in growth rate was probably due to the curvature-related instability. It was shown that mixing enhancement was not greatly reduced if the swirling jets were of a light gas (e.g., hydrogen). When the jet pressure was reduced sufficiently below matched pressure, turbulence was generated in the vortex core by vortex breakdown, providing a second mechanism for mixing enhancement. Thus, the addition of swirl to fuel jets should prove an effective way of enhancing fuel/air mixing in scramjets, even for a light-gas fuel such as hydrogen.

Acknowledgments

We acknowledge financial support from NASA (NCC1-24 and NAS1-18458 Task 1) and the assistance of G. B. Northam and the staff of the NASA Langley Research Center, whose facilities and equipment we used.

References

[1]Papamoschou, D., and Roshko, A.,"Observations of Supersonic Free Shear Layers," AIAA Paper 86-0162, Jan. 1986.

[2]Papamoschou, D., and Roshko, A., "The Compressible Turbulent Shear Layer: An Experimental Study," *Journal of Fluid Mechanics*, Vol. 197, 1988, pp. 453–477.

[3]Fourgette, D., and Dibble, R., "Time Evolution of the Shear Layer of a Supersonic Axisymmetric Jet," *AIAA Journal*, Vol. 29, No. 7, 1991, pp. 1123–1130.

[4]Naughton, J. W., "The Enhancement of Compressible Turbulent Mixing via Streamwise Vorticity," Ph.D. Thesis, Dept. of Mechanical Engineering, Pennsylvania State Univ., University Park, PA, May 1993.

[5]Naughton, J. W., and Settles, G. S., "A Theoretical Framework for Mixing Layers Surrounding Compressible Turbulent Swirling Jets," AIAA Paper 94-2245, June 1994.

[6]Yih, C. S., "Dual Role of Viscosity in the Instability of Revolving Fluids of Variable Density" *Physics of Fluids*, Vol. 4, No. 7, 1961, pp. 806–811.

[7]Khorrami, M. R., "Stability of a Compressible Swirling Jet," AIAA Paper 91-1770, June 1991.

[8]Bradshaw, P., "Effects of Streamline Curvature on Turbulent Flow," AGARDograph 169, Aug. 1973.

[9]Leibovich, S., "Vortex Stability and Breakdown: Survey and Extension," *AIAA Journal*, Vol. 22, No. 9, 1984, pp. 1192–1206.

[10]Gostintsev, A., Zelentsov, V. V., Ilyukhin, V. S., and Pokhil, P. F., "Structure of Underexpanded Supersonic Swirling Gas Jet," *AN SSSR Mekhanika Zhidkosti i Gaza*, Vol. 4, No. 5, 1969, pp. 158–162.

[11]Délery, J., Horowitz, E., Leuchter, O., and Solignac, J.-L., "Fundamental Studies on Vortex Flows," *La Recherche Aérospatiale*, No. 2, 1984, pp. 1–24.

[12]Cattafesta, L. N., and Settles, G. S., "Experiments on Shock/Vortex Interaction," AIAA Paper 92-0315, Jan. 1992.

[13]Kandil, O. A., and Kandil, H. A., "Supersonic Quasi-Axisymmetric Vortex Breakdown," AIAA Paper 91-3311, Sept. 1991.

[14]Clemens, N. T., and Mungal, M. G., "A Planar Mie Scattering Technique for Visualizing Supersonic Mixing Flows," *Experiments in Fluids*, Vol. 11, No. 2/3, 1991, pp. 175–185.

[15]Cutler, A. D., and Levey, B. S., "Vortex Breakdown in a Supersonic Jet," AIAA Paper 91-1815, June 1991.

[16]Savino, J. M., and Ragsdale, R. G., "Some Temperature and Pressure Measurements in Confined Vortex Fields," *Journal of Heat Transfer*, Vol. 83, No. 1, 1961, pp. 33–38.

[17]Deissler, R. G., and Perlmutter, M., "Analysis of the Flow and Energy Separation in a Turbulent Vortex," *International Journal of Heat and Mass Transfer*, Vol. 1, No. 2/3, 1960, pp. 173–191.

[18]Mehta, R. D., Wood, D. H., and Clausen, P. D., "Some Effects of Swirl on Turbulent Mixing Layer Development," *Physics of Fluids A*, Vol. 3, Nov. 1991, pp. 2716–2724.